DR. NICHOLAS GREGORY SMITH (Orcid ID : 0000-0001-7048-4387)

Article type : Primary Research Articles

Title: Mechanisms underlying leaf photosynthetic acclimation to warming and elevated CO_2 as inferred from least-cost optimality theory

Running Head: Photosynthetic acclimation to global change

Nicholas G. Smith[1,2,*], Trevor F. Keenan[2,3]

[1]Department of Biological Sciences, Texas Tech University, Lubbock, TX USA

[2]Climate and Ecosystem Sciences, Lawrence Berkeley National Laboratory, Berkeley, CA USA

[3]Department of Environmental Science, Policy and Management, UC Berkeley, Berkeley, CA USA

[*]Correspondence to:

2901 Main St.

Lubbock, TX 79409

Email: nick.smith@ttu.edu

Phone: 806-834-7363

Abstract

The mechanisms responsible for photosynthetic acclimation are not well understood, effectively limiting predictability under future conditions. Least-cost optimality theory can be used to predict the acclimation of photosynthetic capacity based on the assumption that plants maximize carbon uptake while minimizing the associated costs. Here, we use this theory as a null model in combination with multiple datasets of C_3 plant photosynthetic traits to elucidate the mechanisms

underlying photosynthetic acclimation to elevated temperature and CO_2. The model-data comparison showed that leaves decrease the ratio of the maximum rate of electron transport to the maximum rate of Rubisco carboxylation (J_{max}/V_{cmax}) under higher temperatures. The comparison also indicated that resources used for Rubisco and electron transport are reduced under both elevated temperature and CO_2. Finally, our analysis suggested that plants under-invest in electron transport relative to carboxylation under elevated CO_2, limiting potential leaf-level photosynthesis under future CO_2 concentrations. Altogether, our results show that acclimation to temperature and CO_2 is primarily related to resource conservation at the leaf level. Under future, warmer, high CO_2 conditions, plants are therefore likely to use less nutrients for leaf level photosynthesis, which may impact whole-plant to ecosystem functioning.

Keywords

Photosynthesis, acclimation, climate change, biosphere-atmosphere feedbacks, Rubisco, electron transport, nutrients, V_{cmax}

Introduction

Much of the uncertainty in Earth System Model (ESM) projections of future terrestrial carbon uptake and storage (Friedlingstein *et al.*, 2013) is due to uncertainty in the response of photosynthetic carbon assimilation to future conditions (Booth *et al.*, 2012). Biochemical models of the relative limitations of C_3 photosynthesis have been developed from photosynthetic theory and have proven capable of characterizing the short-term response (i.e., seconds to minutes) of photosynthesis to environmental conditions, such as light, temperature, and CO_2 (Farquhar *et al.*, 1980) . However, the long-term response (i.e., weeks to years) and acclimation of photosynthesis to a changing environment has, to date, been more difficult to suitably characterize for integration into ESMs (Smith & Dukes, 2013; Rogers, 2014; Lombardozzi *et al.*, 2015; Rogers *et al.*, 2017a; Smith *et al.*, 2017).

Across a variety of plant types, the biochemical processes underlying photosynthesis have been shown to acclimate to expected global changes - elevated temperature and CO_2 in particular (Ainsworth & Long, 2005; Ainsworth & Rogers, 2007; Kattge & Knorr, 2007; Leakey *et al.*, 2009; Smith & Dukes, 2013; Dusenge *et al.*, 2019). In response to temperature, photosynthetic biochemical acclimation typically results in an alteration of the instantaneous response of Rubisco carboxylation and electron transport (Smith & Dukes, 2013). This is

commonly observed as a positive shift in the temperature optimum of maximum Rubisco carboxylation (V_{cmax}) and electron transport (J_{max}) rates with warming (Kattge & Knorr, 2007; Scafaro *et al.*, 2017; Smith & Dukes, 2017a). This increase is due to a stimulation of enzymatic activity as well as a change in the thermal stability of the component membranes (Sage & Kubien, 2007), altered production of different Rubisco activase isoforms (Sage & Kubien, 2007; Yamori *et al.*, 2014), and/or the production of different Rubisco subunit isoforms (Hikosaka *et al.*, 2006). Additionally, the sensitivity of acclimated rates of V_{cmax} and J_{max} to temperature tends to be lower than expected from the instantaneous (or kinetic) response (Smith & Dukes, 2013). In addition, the ratio of J_{max} to V_{cmax} (J_{max}/V_{cmax}) is shown to consistently decrease as a result of acclimation to warmer temperatures (Kattge & Knorr, 2007; Smith & Dukes, 2017a, 2018), an effect that is likely in part due to the different shapes of the kinetic temperature response of V_{cmax} and J_{max} (Smith & Dukes, 2017a) as well as a shift in the relative allocation of leaf resources to Rubisco to counteract increased rates of photorespiration at warmer temperatures (Kattge & Knorr, 2007; Scafaro *et al.*, 2017; Smith & Dukes, 2018).

In response to elevated CO_2, photosynthetic acclimation tends to result in reduced stomatal conductance and V_{cmax} (Ainsworth & Rogers, 2007). The reduction in stomatal conductance is thought to be a water saving mechanism and follows predictions from the least-cost theory of stomatal conductance (Wright *et al.*, 2003; Prentice *et al.*, 2014). The mechanisms underlying the reduction of V_{cmax} under elevated CO_2 are not as well understood (Smith & Dukes, 2013). Previous studies have suggested that this reduction may be due to nitrogen (or other nutrient) limitation (Ainsworth & Long, 2005). This follows from the idea that nutrients essential to plant productivity may limit future CO_2 fertilization (Luo *et al.*, 2004; Reich *et al.*, 2006). However, the reduction in V_{cmax} under elevated CO_2 may instead be the result of altered resource investment rather than resource limitation. Because greater CO_2 reduces Rubisco substrate limitation, acclimating plants may be actively investing resources away from CO_2 capture and towards other processes limiting productivity (Leakey *et al.*, 2009).

Empirical formulations have been developed for including photosynthetic capacity acclimation into large-scale models (Smith & Dukes, 2013). Kattge and Knorr (2007) developed a series of empirical formulations for simulating temperature acclimation of V_{cmax} and J_{max} based on a meta-analysis of literature data. These formulations have been shown to increase photosynthesis under future, warmer conditions as compared to simulations that did not include

acclimation (Lombardozzi *et al.*, 2015; Smith *et al.*, 2016, 2017; Mercado *et al.*, 2018) and are being increasingly included into the land surface component of ESMs (e.g., Oleson *et al.*, 2013; Mercado *et al.*, 2018). Recently, updated photosynthetic temperature acclimation formulations using an expanded dataset were produced by Kumarathunge *et al.* (2019).

Acclimation of photosynthetic capacity to elevated CO_2 has traditionally been simulated indirectly, via nitrogen cycle feedbacks (e.g., Thornton et al. 2007). This approach assumes and is reliant on resource limitation to photosynthesis under elevated CO_2. While it has been shown that biomass stimulation by elevated CO_2 is influenced by nitrogen availability (Luo *et al.*, 2004; Reich *et al.*, 2006; Norby *et al.*, 2010), the downregulation of photosynthesis may instead be due to photosynthetic capacity optimization (Haxeltine & Prentice, 1996).

Previous formulations for simulating acclimation to temperature and CO_2 have all been developed using empirical approaches and, in many cases (e.g., Verheijen *et al.*, 2015), without inclusion of any mechanisms. As a result, these models are not likely to produce reliable estimates of future responses, particularly in long simulations that force plants to respond to novel temperature and CO_2 conditions (Prentice *et al.*, 2015), such as those simulated by the Climate Model Intercomparison Project (CMIP). To produce reliable results, model formulations need to be developed from first principles-based knowledge of the underlying biological processes, such that the predictions made regarding the underlying processes can be falsified using measured data.

Recently, a first principles-based theory has been developed for simulating photosynthetic acclimation (Wang *et al.*, 2017a; Smith *et al.*, 2019). The theory is based on the coordination (Maire *et al.*, 2012) and least-cost (Wright *et al.*, 2003; Prentice *et al.*, 2014) photosynthetic optimization theories. The coordination theory states that photosynthetic capacity acclimates in such a way that, under the acclimated conditions, photosynthesis is neither limited by Rubisco carboxylation nor electron transport (Maire *et al.*, 2012). The least-cost theory states that the relative investment in photosynthetic capacity and water transport are optimized such that a given photosynthetic rate is achieved at the lowest cost (Wright *et al.*, 2003). The theory predicts the long-term photosynthetic responses to environmental changes, including elevated temperature and CO_2. It predicts that elevated temperatures will increase V_{cmax}, but that the increase will be less than the short-term kinetic response of V_{cmax} to temperature. The theory also predicts a decrease in the ratio of J_{max} to V_{cmax} (J_{max}/V_{cmax}) with increasing temperatures. In

response to elevated CO_2, the theory predicts a decrease in V_{cmax}, resulting in an increase in J_{max}/V_{cmax}. This theory has been shown to reliably predict the current distribution of global photosynthetic capacity (Wang *et al.*, 2017a; Smith *et al.*, 2019). However, it has not been tested in terms of its capacity to predict responses to expected future global changes.

Here, we leverage data from climate manipulation experiments to examine whether photosynthetic capacity (i.e., V_{cmax} and J_{max}) acclimates to elevated temperature and CO_2 as expected from optimization. The results of this model-data comparison are used to gain insight into the mechanisms influencing leaf-level photosynthetic responses to future conditions.

Materials and Methods

Theoretical model of optimal photosynthesis

To predict optimal rates of V_{cmax} and J_{max}, we combined the optimal theory of photosynthetic coordination (Maire *et al.*, 2012) with an optimal stomatal conductance model (Prentice *et al.*, 2014), as in Smith *et al.* (2019). The primary assumption of the combined model comes from least-cost theory of photosynthesis (Wright *et al.*, 2003). This assumption is that, optimally, leaf-level photosynthesis will operate at the fastest rate for a given environment while using the least amount of resources, namely water and nitrogen (Wright *et al.*, 2003).

The optimal photosynthesis theory assumes that plants will coordinate their photosynthetic machinery such that the rate of Rubisco carboxylation-limited photosynthesis (A_c) is equal to that of electron transport rate-limited photosynthesis (A_j) under typical environmental conditions (Maire *et al.*, 2012):

$$A_c = A_j \quad (1)$$

Using photosynthetic biochemical theory (Farquhar *et al.*, 1980), optimal V_{cmax}, J_{max}, and J_{max}/V_{cmax} can then be derived as

$$V_{cmax} = \varphi I\left(\frac{m}{m_c}\right)\left(\frac{\varpi^*}{8\theta}\right) \quad (2)$$

$$J_{max} = \varphi I \varpi \quad (3)$$

$$\frac{J_{max}}{V_{cmax}} = \frac{8\theta m_c \varpi}{m\varpi^*} \quad (4)$$

where φ (mol mol^{-1}) is the realized quantum yield of photosynthetic electron transport, I (μmol m^{-2} s^{-1}) is the incident photosynthetically active photon flux density, m (Pa Pa^{-1}) is the Michaelis-Menten term that describes the limitation of A_j by intracellular CO_2 (C_i; Pa), m_c (Pa Pa^{-1}) is the

Michaelis-Menten term that describes the limitation of A_c by intracellular CO_2 (C_i; Pa), θ (unitless) is the curvature of the light response curve, and ω and ω* are terms that describe the cost to maintain electron transport. In the model, C_i is calculated using the optimal stomatal conductance model derived by Prentice *et al.* (2014), which assumes that rates of conductance maximize photosynthesis while minimizing water loss and nutrient use. Specifically, the model solves for the optimal ratio (χ) of C_i to atmospheric CO_2 partial pressure (C_a; Pa):

$$\chi = \frac{\Gamma^*}{C_a} + \left(1 - \frac{\Gamma^*}{C_a}\right)\frac{\xi}{\xi + \sqrt{D}} \quad (5)$$

where Γ* is the CO_2 compensation point in the absence of mitochondrial respiration (Pa), D is leaf-to-air vapor pressure deficit (Pa) and

$$\xi = \sqrt{\beta \frac{K + \Gamma^*}{1.6\eta^*}} \quad (6)$$

where K is the Michaelis-Menten coefficient for Rubisco (Pa), η^* is the viscosity of water relative to its value at 25°C (unitless), calculated using temperature and elevation as in Huber *et al.* (2009), and β is the ratio of the cost to maintain carboxylation to the cost to maintain transpiration, estimated as 146 under standard conditions (T_g = 25˚C, D_g = 1 kPa, z = 0) from an analysis of leaf stable carbon isotope data (Wang *et al.*, 2017a). The full derivation of the model is included in the supplementary information, but is briefly described here. The full model code is published at https://github.com/smithecophyslab/optimal_vcmax_r/releases/tag/v2.1 (DOI: 10.5281/zenodo.3874938).

Pertinent to this study is the predicted optimal acclimation of V_{cmax}, J_{max}, and J_{max}/V_{cmax} to temperature and atmospheric CO_2. The m and m_c terms are sensitive to temperature and CO_2. This is also true of ω and ω*, which are both direct functions of m (see supplementary materials). Both m and m_c are calculated using Γ*, which increases exponentially with temperature (Bernacchi *et al.*, 2001). Additionally, m is calculated using Michaelis-Menten terms for Rubisco carboxylation and oxygenation, which also increase exponentially with temperature (Bernacchi *et al.*, 2001). Additionally, the C_i calculation (equation 5) includes temperature-dependent terms Γ* (Bernacchi *et al.*, 2001), K (Bernacchi *et al.*, 2001), and η* (Huber *et al.*, 2009). The CO_2 response is dictated by the response of C_i to CO_2 (equation 5), which then modifies the m and m_c terms in equations 2-4, as well as the ω and ω*, due to the fact that they are direct functions of m. Notably, these responses are based on theoretical formulations described above, but do rely on

empirical assumptions of the temperature response of Γ* (Bernacchi *et al.*, 2001), *K* (Bernacchi *et al.*, 2001), and η* (Huber *et al.*, 2009).

Observational datasets

V_{cmax} and J_{max} temperature acclimation data were taken from Smith and Dukes (2017a) and Scafaro *et al.* (2017). We used these data because they examined temperature acclimation within a single experiment and, as such, did not confound acclimation (the response of single individual as the result of phenotypic plasticity) and adaptation (the response over multiple generations) responses. Data from Smith and Dukes (2017a) were extracted from GitHub (https://github.com/SmithEcophysLab/PU_GrowthChamber; doi: 10.5281/zenodo.1181729). V_{cmax} data from Scafaro *et al.* (2017) was extracted directly from figures in the paper using WebPlotDigitizer version 4.0 (Rohatgi, 2017). Notably, data for J_{max} could not be extracted for Scafaro *et al.* (2017). Environmental data necessary for running the theoretical model were taken from information contained in the paper.

For comparison of temperature responses in observational data, we used a global observational dataset of open access V_{cmax} and J_{max} values, similar to the one used in Smith *et al.* (2019). This was built by combining independent data reported to be from top canopy, natural vegetation from Domingues *et al*. (2010), Domingues *et al*. (2015), Keenan & Niinemets (2016), Maire *et al.* (2015), Niinemets *et al.* (2015), Rogers *et al.* (2017b), Smith & Dukes (2017a), Togashi *et al*. (2018a), Togashi *et al*. (2018b), the TRY plant trait database (Kattge *et al.*, 2011, 2020), and Wang *et al.* (2017a). Data were chosen based on whether values necessary to fit the optimal photosynthesis model were reported or could be reasonably estimated (e.g., climate data; see below). One notable reason why data were omitted was the lack of a reported leaf temperature at which measurements were taken. Latitude and longitude were used to extract effective growing season mean temperature (T_g; °C), atmospheric vapor pressure deficit (D_g; Pa), and incoming photosynthetically active radiation (I_g; μmol m^{-2} s^{-1}) for each site from monthly, 1901-2015, 0.5° resolution data provided by the Climatic Research Unit (CRU TS3.24.01) (Harris *et al.*, 2014). Growing season was operationally defined as months with mean temperatures greater than 0°C. The elevation (z; m) at each site at 0.5° resolution was obtained from the WFDEI meteorological forcing dataset (Weedon *et al.*, 2014).

Two previous studies have developed empirical formulations to describe the temperature acclimation of V_{cmax}, J_{max}, and the J_{max}/V_{cmax} ratio as observed in global datasets (Kattge & Knorr, 2007; Kumarathunge *et al.*, 2019). As such, these formulations serve as an additional temperature response dataset to compare against. These models are modifications of the Arrhenius equation describing the instantaneous response of V_{cmax} and J_{max} to leaf temperature:

$$f(T) = e^{\frac{H_a(T_{leaf} - 298.15)}{RT_g 298.15}} \frac{1 + e^{\frac{298.15(\Delta S) - H_d}{R298.15}}}{1 + e^{\frac{T_{leaf}(\Delta S) - H_d}{RT_{leaf}}}} \quad (7)$$

and

$$k_{Tleaf} = k_{25} f(T) \quad (8)$$

where k is the rate of V_{cmax} or J_{max} at the leaf temperature (k_{Tleaf}) or at 25°C (k_{25}), H_a is the activation energy (J mol^{-1}), R is the universal gas constant (8.314 J mol^{-1} K^{-1}), H_d is the deactivation energy (200,000 J mol^{-1}), and ΔS is the entropy term that characterizes the changes in reaction rate caused by substrate concentration (J mol^{-1} K^{-1}). To incorporate temperature acclimation, the two studies use observational data to describe the linear response of ΔS, H_a, and k_{25} to temperature (see Table 1). We included these two empirical temperature acclimation formulations into our comparison by calculating V_{cmax}, J_{max}, and the J_{max}/V_{cmax} ratio at leaf temperature (T_{leaf}) equal to the acclimated temperature (T_{acc}) across the temperature range from our global observational dataset (3-30°C).

A summary of all datasets used for temperature response comparisons can be found in Table S2.

Carbon dioxide (CO_2) acclimation data were obtained via a Google Scholar literature search using keywords "elevated CO_2" and "V_{cmax}," resulting in data from 31 studies examining photosynthetic biochemistry under elevated CO_2 (Ziska *et al.*, 1991; Harley *et al.*, 1992; McKee & Woodward, 1994; McKee *et al.*, 1995; Curtis *et al.*, 1995; Osborne *et al.*, 1998; Rey & Jarvis, 1998; Rogers *et al.*, 1998; Sims *et al.*, 1998; Turnbull *et al.*, 1998; Li *et al.*, 1999; Medlyn *et al.*, 1999; Myers *et al.*, 1999; Tissue *et al.*, 1999; Davey *et al.*, 1999; Adam *et al.*, 2000; Griffin *et al.*, 2000; Von Caemmerer *et al.*, 2001; Hovenden, 2003; Zhao *et al.*, 2004; Ellsworth *et al.*, 2004; Kitao *et al.*, 2007; Yong *et al.*, 2007; Crous *et al.*, 2010; Yu *et al.*, 2012; Ge *et al.*, 2012; Hao *et al.*, 2012; Blumenthal *et al.*, 2013; Warren *et al.*, 2015; Sharwood *et al.*, 2017; Aspinwall *et al.*, 2018). As with the temperature response dataset, data for CO_2 acclimation were chosen

based on whether values necessary to fit the optimal photosynthesis model were reported or could be reasonably estimated (e.g., climate data; see below). One notable reason why data were omitted was the lack of a reported leaf temperature at which measurements were taken. Data obtained were mean and reported error values under the low and high CO_2 environments. In cases where data were not presented in tables, data from figures were extracted using WebPlotDigitizer version 4.0 (Rohatgi, 2017). Where available, environmental data necessary for running the model (e.g., temperature and vapor pressure deficit) were extracted from individual papers. This was true for all controlled environment studies. In cases where environmental data were not reported, latitude and longitude were used to extract effective growing season mean temperature (T_g), atmospheric vapor pressure deficit (D_g), and incoming photosynthetically active radiation (I_g) for each site from monthly, 1901-2015, 0.5° resolution data provided by the Climatic Research Unit (CRU TS3.24.01) (Harris *et al.*, 2014). Growing season was defined as months with average temperatures greater than 0°C. The elevation (z) at each site at 0.5° resolution was obtained from the WFDEI meteorological forcing dataset (Weedon *et al.*, 2014). In all cases, we averaged species-specific and/or time-specific responses for each 0.5° resolution site in order to not bias sites where more species or time points were reported. In total, our dataset included 51 species from 33 elevated CO_2 sites, with 115 unique species by site combinations. Note that 21 of 115 species by site combinations did not report J_{max} values (all reported V_{cmax} values). The full dataset included studies that utilized free air CO_2 enrichment (FACE; n = 12), open top chambers (OTCs; n = 11), whole-tree chambers (WTCs; n = 1), and controlled environment chambers (CEs; n = 9).

A summary of the data used for the CO_2 response comparisons can be found in Table S2.

Model-data comparison

The optimal acclimation model predicts acclimation of photosynthetic capacity and investment in different biochemical processes via V_{cmax} (equation 2), J_{max} (equation 3), and their ratio (J_{max}/V_{cmax}; equation 4). We compared the temperature response of the optimality predicted V_{cmax}, J_{max}, and J_{max}/V_{cmax} to that observed in an acclimation-only studies by Smith and Dukes (2017a) and Scafaro *et al.* (2017). As part of this comparison, we also included the response predicted by instantaneous enzyme kinetics (i.e., no acclimation), using unacclimated, mean parameters from Kattge and Knorr (2007) (Table 1). We made the comparisons by calculating

predicted optimal and kinetic values for J_{max} and V_{cmax} for each value in both datasets using reported values for environmental variables for the Smith and Dukes (2017a) and Scafaro *et al.* (2017) datasets. We then computed slopes of the relationship between the acclimated temperature (independent variable) and the natural log transformed values of V_{cmax}, J_{max}, and J_{max}/V_{cmax} (dependent variables) for the observations, kinetic model, and optimality model using the 'lm' function in R (R Core Team, 2019). We then compared the slopes calculated from the observations, kinetic model, and optimality model to each other.

We also compared optimality and kinetic predicted values to those observed in the global observational dataset as well as those produced from the empirical models developed from global observational data by Kattge and Knorr (2007) and Kumarathunge *et al*. (2019). We did this by calculating predicted optimal and kinetic values for J_{max} and V_{cmax} for each value in both datasets using estimated values for the global observational dataset. We then computed slopes of the relationship between the acclimated temperature (independent variable) and the natural log transformed values of V_{cmax}, J_{max}, and J_{max}/V_{cmax} (dependent variables) for the observations and observation-based models, kinetic model, and optimality model using the 'lm' function in R (R Core Team, 2019). We finally compared the slopes calculated from the observations and observation-based models, kinetic model, and optimality model to each other.

For the CO_2 acclimation-only data, we used the optimality model to compute optimal V_{cmax}, J_{max}, and J_{max}/V_{cmax} values for each species at each site. We then calculated the slope of natural log response of V_{cmax}, J_{max}, and J_{max}/V_{cmax} (dependent variables) to CO_2 (independent variable) for the observations and the optimal photosynthesis model. We then compared slopes from the observations and the optimal photosynthesis model to each other. Finally, we used a linear model to explore whether differences between the data and the optimal photosynthesis model were explained by temperature, light, vapor pressure deficit, elevation, or the elevated CO_2 methodology employed. In our model, we also considered mycorrhizal association for each species by site combination, as this was found to influence photosynthetic capacity responses to elevated CO_2 in a previous study (Terrer *et al.*, 2018). Specifically, we grouped each species by whether they associate with arbuscular mycorrhizal fungi (AM, n = 60 for all species by site combinations and n = 44 for species by site combination that reported J_{max}), ectomycorrhizal fungi (EM, n = 46 for all species by site combinations and n = 43 for species by site combination that reported J_{max}), or nitrogen fixing bacteria (NF, n = 12 for all species by site combinations

and n = 9 for species by site combination that reported J_{max}), or if the individuals were given nitrogen fertilization (n = 8 for all species by site combinations and n = 4 for species by site combination that reported J_{max}). Nitrogen acquisition data were obtained at the species level using prior reports on mycorrhizal and nitrogen-fixing bacteria symbioses. Note that some EM and NF associating species may be able to also associate with AM fungi. Species were considered NF or EM if they were known to associate with those respective symbionts and regardless of whether they associate with AM fungi. Specifically, the linear model included the difference in CO_2 sensitivity between the optimal photosynthesis model and the observations as the dependent variable and temperature, light, vapor pressure deficit, elevation, the elevated CO_2 methodology employed, and nitrogen acquisition as independent variables. To address the fact that some variables in the model are inherently correlated, we calculated generalized variance inflation factors for each independent variable in each model (Zuur *et al.*, 2009) using the 'car' package (Fox & Weisberg, 2011) in R (R Core Team, 2019). In all cases, the generalized variance inflation factors were less than 3, indicating that collinearity had little impact on the results (Zuur *et al.*, 2009).

Per leaf area optimal nitrogen in Rubisco simulations

To explore how leaf nitrogen would be expected to change under different temperature and CO_2 conditions, we calculated an estimate of leaf nitrogen in Rubisco and leaf nitrogen in bioenergetics from V_{cmax} and J_{max}, respectively, under different temperatures and CO_2 concentrations. Specifically, we used equation 12 to simulate V_{cmax} under a combination of 4 acclimated temperatures ranging from 5-35°C and 7 acclimated atmospheric CO_2 concentrations from 400-1000 ppm. These simulations were done using both a low (1 kPa) and high (6 kPa) vapor pressure deficit. All simulations were done at an elevation of 0 m and acclimated light level of 1000 μmol m^{-2} s^{-1}. V_{cmax} and J_{max} values were then converted to temperature standardized values at 25°C ($V_{cmax,25}$ and $J_{max,25}$, respectively) using equations 18 and 19 and parameterizations of Kattge and Knorr (2007). The $V_{cmax,25}$ values were then used to estimate leaf nitrogen in Rubisco per unit area ($N_{rubisco}$) following the approach by Dong *et al*. (2017), based on the model and parameterizations of Harrison *et al.* (2009):

$$N_{rubisco} = \frac{V_{cmax,25} M_r M_n [N_r]}{k_{cat} n_r} \quad (9)$$

where M_r is the molecular mass of Rubisco, 0.55 g Rubisco (μmol Rubisco)$^{-1}$, [N_r] is the nitrogen concentration of Rubisco, 0.0144 mol nitrogen (g Rubisco)$^{-1}$, M_n is the molecular mass of nitrogen, 14 g nitrogen (mol nitrogen)$^{-1}$, k_{cat} is the catalytic turnover at 25°C, 3500000 μmol CO_2 (mol Rubisco sites * seconds)$^{-1}$, and n_r is the catalytic sites per mol Rubisco, 8 mol sites (mol Rubisco)$^{-1}$. The $J_{max,25}$ values were used to estimate nitrogen in bioenergetics ($N_{bioenergetics}$) following the approach by Niinemets and Tenhunen (1997):

$$N_{bioenergetics} = \frac{J_{max,25} N_{cyt}}{j_{mc}} \quad (10)$$

where N_{cyt} is the nitrogen investment in bioenergetics (0.124 gN (μmol cyt f)$^{-1}$) and j_{mc} is the activity of electron transport at 25°C (156 μmol e$^-$ (μmol cyt f * s)$^{-1}$) (Niinemets & Tenhunen, 1997). Photosynthetic nitrogen was computed by adding $N_{rubisco}$ and $N_{bioenergetics}$.

Results

Temperature responses

The optimal temperature response of the J_{max}/V_{cmax} ratio (natural log transformed slope ± 95% CI: -0.051 ± 0.001 °C^{-1}; Table 2 and Fig. 1a) was similar to that observed in a growth chamber study (Smith and Dukes 2017a; -0.048 ± 0.012 °C^{-1}; Table 2 and Fig. 1a). Notably, this response was much steeper than the response predicted from the enzyme kinetic responses of J_{max} and V_{cmax} alone (-0.028 ± 0.0005 °C^{-1}; Table 2 and Fig. 1a). However, the optimal temperature responses of J_{max} and V_{cmax} were shallower than those observed (Table 2, Fig. 1b, and Fig. 1c). As the J_{max} and V_{cmax} responses are dependent on φ, this discrepancy likely indicates that the temperature response of φ in our model was weaker than the temperature response of φ in the data (equation 15). The J_{max}/V_{cmax} ratio is independent of φ.

The similarity between the slope of the optimal temperature response of the J_{max}/V_{cmax} ratio (-0.041 ± 0.0001 °C^{-1}; Table 3 and Fig. 2a) and that observed in the global observational dataset (-0.046 ± 0.002 °C^{-1}; Table 3 and Fig. 2a) and observation-based models of Kattge and Knorr (2007) (-0.041 ± 0.002 °C^{-1}; Table 3 and Fig. 2a) and Kumarathunge *et al*. (-0.032 ± 0.001 °C^{-1}; Table 3 and Fig. 2a) suggest that plants were setting up their photosynthetic biochemistry optimally in response to temperature. Nonetheless, slightly weaker temperature responses of J_{max} and V_{cmax} in the optimal model indicate a lack of full agreement between the optimal model and data (Table 3, Fig. 2b, and Fig. 2c). As with the growth chamber data comparison, this is likely

driven by inadequate parameterization of φ or with biased estimates of leaf canopy light availability, both of which influence J_{max} and V_{cmax}, but not the ratio of the two.

Elevated CO_2 response

On average, the observed natural log slope of the response of V_{cmax} to CO_2 (mean ± 95% CI: -0.0056 ± 0.0018 Pa^{-1}) was similar to that predicted by the optimality model (-0.0061 ± 0.0002 Pa^{-1}). However, the observed J_{max} response was negative (-0.0034 ± 0.0016 Pa^{-1}), while the optimal predicted response was positive (0.0022 ± 0.0001 Pa^{-1}). This led to an increase in the J_{max}/V_{cmax} ratio that was lower in the observed data (0.0018 ± 0.0015 Pa^{-1}) than was predicted by optimization (0.0083 ± 0.0004 Pa^{-1}).

We calculated the difference in the log regression slopes for each species in each experiment from that expected by optimization to explore potential drivers of this difference. Specifically, we examined influences of temperature, light availability, vapor pressure deficit, elevation, nitrogen acquisition strategy, and methodology used by the experiment. Of those, only nitrogen acquisition strategy had a significant influence on the bias between the modeled and observed CO_2 responses (Table 4 and Fig. 3). In fact, the slope of the observed response of J_{max}/V_{cmax} to CO_2 was 9 times larger in species with associations with nitrogen fixing bacteria (NF) than in species that only have associations with fungi (AM or EM; Table 5 and Fig. 3a). The slope of the response of J_{max}/V_{cmax} to CO_2 for NF species was nearly identical to that predicted by optimality (Table 5 and Fig. 3a), indicating that species with strictly fungal associations were underinvesting in J_{max} under elevated CO_2. This was confirmed by comparing the response of V_{cmax} and J_{max} separately, analyses that indicated the V_{cmax} response was near optimal in all species (Table 5 and Fig. 3b), but the J_{max} response was suboptimal in AM and EM species (Table 5 and Fig. 3c). However, results from nitrogen fertilization experiments also had low J_{max}/V_{cmax} slopes (Table 5).

Predicted Leaf nitrogen response from warming and elevated CO_2 acclimation

Given the strong responses of photosynthetic capacity to warming and elevated CO_2 predicted by least-cost optimality and observed in empirical studies, we explored how this acclimation would impact leaf nitrogen content. We used the optimality model described above in concert with models that estimate leaf nitrogen in Rubisco and bioenergetics from V_{cmax} and

J_{max}, respectively (see Methods). We found a consistent decrease in photosynthetic nitrogen under both warming and elevated CO_2 and regardless of atmospheric VPD (Fig. 4). Both the temperature- and CO_2-driven downregulation was stronger at low temperatures and low CO_2 (Fig. 4).

Discussion

Photosynthetic capacity acclimation to future increases in CO_2 and temperature will influence the rate and magnitude of future climate change (Galbraith *et al.*, 2010; Smith & Dukes, 2013). Past studies have reviewed photosynthetic capacity acclimation to elevated CO_2 (Ainsworth & Long, 2005; Ainsworth & Rogers, 2007; Leakey *et al.*, 2009) and temperature (Kattge & Knorr, 2007; Yamori *et al.*, 2014; Kumarathunge *et al.*, 2019). Nonetheless, uncertainties regarding the mechanisms underlying these responses has led to a limited inclusion of these processes in Earth System Models (Smith & Dukes, 2013). Plant-centric models of photosynthesis have indicated that the acclimation of the biochemical processes underlying photosynthesis may be the result of optimal coordination, under which plants set up their biochemistry in order to maintain high rates of photosynthesis at the lowest possible nutrient use (Maire *et al.*, 2012; Wang *et al.*, 2017a; Smith *et al.*, 2019). Here, we explicitly test this theory using published observational and manipulative data to elucidate the mechanisms underlying acclimation responses. We discuss each of the primary findings below; namely, that (1) biochemical acclimation to increasing temperatures in C_3 plants increases maximum rates of Rubisco carboxylation relative to electron transport, (2) leaves acclimate to temperature and CO_2 by reducing per-leaf-area nutrient use, and (3) photosynthesis is restricted by a suboptimal response of electron transport under elevated CO_2.

Warm temperature acclimation in C_3 plants increases maximum rates of Rubisco carboxylation relative to electron transport

In response to elevated temperatures, the C_3 plants evaluated here increased investment in Rubisco carboxylation relative to electron transport, an effect seen in previous meta-analyses (Kattge & Knorr, 2007; Kumarathunge *et al.*, 2019). As this response was similar to that expected from the optimization model, we can more closely investigate the underlying mechanism. The parameters responsible for the predicted decrease, shown in equation 14, are ϖ,

ϖ^*, m, and m_c. Note that the ω and ω* are temperature sensitive because they are derived from m. Each of these parameters decreases with increasing temperature. For all parameters, this is a result of an increase in the CO_2 compensation point (Γ^*) with temperature, which is directly related to the increased specificity of Rubisco to O_2 relative to CO_2 with increased temperatures (Bernacchi *et al.*, 2001). The parameter K which describes the Michaelis-Menten coefficients of Rubisco activity for CO_2 and O_2 (see Support Information) also increases with temperature as a result of the greater sensitivity of Rubisco oxygenation relative to carboxylation to temperature, further reducing m_c as temperatures rise. While all four parameters decrease with temperature, the decrease in $\varpi^* m_c$ is greater than that of ϖm due to the stronger dependence of carboxylation (i.e., $\varpi^* m_c$) on Rubisco kinetics than electron transport (i.e., ϖm). This indicates that photorespiration is a primary driver of the acclimation of photosynthetic biochemistry to temperature seen here and in other studies (Kattge & Knorr, 2007; Kumarathunge *et al.*, 2019).

Notably, the temperature responses for V_{cmax} and J_{max} predicted from the optimality model differed slightly from those observed in the temperature manipulation and observational datasets. One possible reason for this is the empirical parameterization of the temperature response of the realized quantum yield of photosynthetic electron transport (φ) in the model (see Supporting Information). A change in the parameterization of this equation would allow us to match the temperature sensitivity. However, we opted against this sort of tuning to avoid biasing our model. Nonetheless, there is very little data on the temperature response of φ in the literature, with very few studies reporting these parameters (Bernacchi *et al.*, 2003; Dongsansuk *et al.*, 2013). Given the model sensitivity to φ and the easy by which it can be measured using fluorometry, more empirical studies estimating its temperature sensitivity under varying ecological conditions would be beneficial to model development.

Leaves acclimate by reducing per leaf nutrient use

Our results indicate that leaves acclimate to both elevated temperatures and CO_2 by reducing their leaf nutrient use. While we did not have nutrient or enzyme content data to test this directly, this reduction can be gleaned directly from the model-data comparison. Under elevated temperature, the dampened response of acclimated V_{cmax} and J_{max} to temperature relative to the kinetic response indicates that these rates at a standard temperature, a common indicator of active photosynthetic protein content (Rogers, 2014), would decrease with increased

temperatures, as suggested in previous studies (e.g., Kattge & Knorr, 2007; Ali *et al.*, 2015; Smith & Dukes, 2018). The agreement between the data and optimization model indicate that this reduction in protein is related to the fact that, at higher temperatures, enzymes work faster, reducing the amount of enzymes needed to assimilate at the optimal rate.

Under elevated CO_2, our data indicated an average decrease in V_{cmax} and J_{max} at higher CO_2 concentrations. The V_{cmax} response was similar to that expected by the optimization model, indicating that this effect was the result of increased substrate for Rubisco (i.e., CO_2) reducing the amount of Rubisco needed to assimilate at the optimal rate. Interestingly, the reduction in J_{max} seen in the elevated CO_2 data was not predicted by the optimization model, possibly indicating a nutrient limitation response (Luo *et al.*, 2004; see discussion below).

The close relationship between the observed V_{cmax} responses and those predicted by the optimization model suggest that plants are acclimating such that leaf biochemistry adjusts so as to fix the greatest amount of carbon at lowest possible nutrient use, a primary tenant of the least cost hypothesis (Wright *et al.*, 2003). With increased temperatures and CO_2 concentration, the per leaf area nutrient use efficiency is increased. This leaf-level response may have multiple resulting benefits at the whole-plant level. Namely, other nutrients could be used to increase growth of new tissue or be stored. This would also reduce nutrient demand, resulting in a decrease in root growth and carbon exudation per unit leaf area. While past studies have examined these total costs under future conditions (e.g., Phillips *et al.*, 2012), future studies should consider these responses relative to carbon uptake by leaves.

Photosynthesis is restricted by electron transport rate under elevated CO_2

Previous studies examining photosynthetic biochemistry responses to elevated CO_2 have interpreted reductions in V_{cmax} that coincide with reductions in leaf nitrogen as indicators of progressive nitrogen limitation (e.g., Ainsworth & Long, 2005; Crous *et al.*, 2008). However, our V_{cmax} results indicate that V_{cmax} is down-regulated as would be expected from optimization alone. Interestingly, however, the lack of agreement between the optimal and observed J_{max} response indicates that plants at elevated CO_2 are more restricted by electron transport than by carboxylation.

Medlyn (1996), utilizing a similar approach to the one used here, reported a similar mismatch between optimal nitrogen allocation to J_{max} and V_{cmax} properties. This discrepancy was

hypothesized to be the result of non-acclimating χ or light regime. Here, we use an optimally acclimating χ, but consider only stomatal and not mesophyll conductance. However, previous work indicates that there is no effect of elevated CO_2 on the relationship between intercellular and mesophyll CO_2 concentration (Singsaas *et al.*, 2004). Light is also not likely to be a factor, as light availability has little effect on J_{max}/V_{cmax} in observations (Poorter *et al.*, 2019) and no effect on our optimization model. Alternatively, the decreased J_{max} could indicate a nitrogen limitation to photosynthesis as expected under the progressive nitrogen limitation hypothesis (Luo *et al.*, 2004). Our, admittedly limited, data from nitrogen fertilization experiments did not indicate that this was the case. There is a strong correlation between J_{max} and V_{cmax} (Walker *et al.*, 2014), so changes in one parameter may result in consequent changes in the other (Onoda *et al.*, 2009), however flexibility in the J_{max}/V_{cmax} ratio would suggest this is not the case. Other environmental variables (e.g., temperature (Wang *et al.*, 2017a)) have been suggested as reasons for this effect, but our bias analyses found no supporting evidence.

The one factor that was indicated by our bias analysis to potentially have an impact on the non-optimal J_{max} response was the association with belowground microorganisms. Previous work has indicated that leaf- and whole-plant level responses to elevated CO_2 are influenced by soil microbial symbioses, specifically the return of nitrogen per carbon invested via belowground allocation to symbionts (Terrer *et al.*, 2016, 2018). Species that primarily associated with soil fungi, and arbuscular mycorrhizal fungi in particular, tend to have lower returns on investment than species that associate with nitrogen fixing bacteria, limiting carbon uptake and growth stimulation under elevated CO_2 in fungal associating species (Terrer *et al.*, 2018). Our study also found evidence of this response, in that species associating with nitrogen fixing bacteria did not show a downregulation of J_{max} under elevated CO_2 and, instead, showed a response similar to that expected from optimization. On the other hand, species with primarily fungal associations showed a response consistent with photosynthetic limitation by electron transport.

However, unlike the results found by Terrer *et al*. (2018), we did not find that nitrogen acquisition strategy was related to V_{cmax} acclimation. Also, we did not find that the electron transport rate limitation was alleviated by added nitrogen. However, these results were based on only a small number of studies; only four studies with fertilization reported J_{max} and only 9 studies were done using species with associations with nitrogen fixing bacteria. Nonetheless, the differential response to elevated CO_2 in species with different nitrogen acquisition strategies

indicates the need to further investigate the role of aboveground-belowground interactions in altering future responses. As demonstrated by Terrer *et al*. (2018), the whole-plant response may be more dependent on these symbioses than leaf-level responses. Future studies, possibly utilizing labeled carbon and nitrogen, could help further explore these mechanisms.

Our results indicate that plants will acclimate their leaf biochemistry in response to future changes in temperature and atmospheric CO_2. This will manifest itself in lower nutrient use for photosynthetic processes at the leaf level. However, at least in the case of responses to elevated CO_2, this may not be a fully optimal response, as the optimization seemed to be limited by the mechanism of nutrient acquisition in some studies and species. These results should be used to explore the consequences of acclimation for whole-plant and ecosystem-level responses, which are less certain, but important for predicting future biosphere-atmosphere feedbacks.

Acknowledgements

NGS acknowledges support from Texas Tech University. NGS and TFK were supported by the Laboratory Directed Research and Development (LDRD) fund under the auspices of DOE, BER Office of Science at Lawrence Berkeley National Laboratory.

Author contributions

NGS and TFK designed the study. NGS performed the analyses. NGS wrote the manuscript with input from TFK.

Data Sharing and Data Accessibility

This study used only previously published data and model code, for which the corresponding citations are noted within the manuscript. We request that users refer to the original studies and cite those accordingly.

References

Adam NR, Wall GW, Kimball BA et al. (2000) Acclimation response of spring wheat in a free-air CO2 enrichment (FACE) atmosphere with variable soil nitrogen regimes. 1. Leaf position and phenology determine acclimation response. *Photosynthesis Research*, **66**, 65–77.

549 Ainsworth EA, Long SP (2005) What have we learned from 15 years of free-air CO2 enrichment
550 (FACE)? A meta-analytic review of the responses of photosynthesis, canopy properties and
551 plant production to rising CO2. *New Phytologist*, **165**, 351–372.
552 Ainsworth EA, Rogers A (2007) The response of photosynthesis and stomatal conductance to
553 rising [CO2]: mechanisms and environmental interactions. *Plant, Cell & Environment*, **30**,
554 258–270.
555 Ali AA, Xu C, Rogers A et al. (2015) Global-scale environmental control of plant photosynthetic
556 capacity. *Ecological Applications*, **25**, 2349–2365.
557 Aspinwall MJ, Blackman CJ, de Dios VR et al. (2018) Photosynthesis and carbon allocation are
558 both important predictors of genotype productivity responses to elevated CO2 in Eucalyptus
559 camaldulensis. *Tree Physiology*, tpy045–tpy045.
560 Bernacchi CJ, Singsaas EL, Pimentel C, Portis Jr AR, Long SP (2001) Improved temperature
561 response functions for models of Rubisco-limited photosynthesis. *Plant, Cell &*
562 *Environment*, **24**, 253–259.
563 Bernacchi CJ, Pimentel C, Long SP (2003) In vivo temperature response functions of parameters
564 required to model RuBP-limited photosynthesis. *Plant, Cell & Environment*, **26**, 1419–
565 1430.
566 Blumenthal DM, Resco V, Morgan JA et al. (2013) Invasive forb benefits from water savings by
567 native plants and carbon fertilization under elevated CO2 and warming. *New Phytologist*,
568 **200**, 1156–1165.
569 Booth BBB, Chris DJ, Mat C et al. (2012) High sensitivity of future global warming to land
570 carbon cycle processes. *Environ. Res. Lett.*, **7**, 24002.
571 Von Caemmerer S, Ghannoum O, Conroy JP, Clark H, Newton PCD (2001) Photosynthetic
572 responses of temperate species to free air CO2 enrichment (FACE) in a grazed New
573 Zealand pasture. *Functional Plant Biology*, **28**, 439–450.
574 Crous KY, Walters MB, Ellsworth DS (2008) Elevated CO2 concentration affects leaf
575 photosynthesis–nitrogen relationships in Pinus taeda over nine years in FACE. *Tree*
576 *Physiology*, **28**, 607–614.
577 Crous KY, Reich PB, Hunter MD, Ellsworth DS (2010) Maintenance of leaf N controls the
578 photosynthetic CO2 response of grassland species exposed to 9 years of free-air CO2
579 enrichment. *Global Change Biology*, **16**, 2076–2088.

Curtis PS, Vogel CS, Pregitzer KS, Zak DR, Teeri JA (1995) Interacting effects of soil fertility and atmospheric CO2 on leaf area growth and carbon gain physiology in Populus× euramericana (Dode) Guinier. *New Phytologist*, **129**, 253–263.

Davey PA, Parsons AJ, Atkinson L, Wadge K, Long SP (1999) Does photosynthetic acclimation to elevated CO2 increase photosynthetic nitrogen-use efficiency? A study of three native UK grassland species in open-top chambers. *Functional Ecology*, **13**, 21–28.

Domingues TF, Meir P, Feldpausch TR et al. (2010) Co-limitation of photosynthetic capacity by nitrogen and phosphorus in West Africa woodlands. *Plant, Cell & Environment*, **33**, 959–980.

Domingues TF, Ishida FY, Feldpausch TR et al. (2015) Biome-specific effects of nitrogen and phosphorus on the photosynthetic characteristics of trees at a forest-savanna boundary in Cameroon. *Oecologia*, **178**, 659–672.

Dong N, Prentice IC, Evans BJ, Caddy-Retalic S, Lowe AJ, Wright IJ (2017) Leaf nitrogen from first principles: field evidence for adaptive variation with climate. *Biogeosciences*, **14**, 481–495.

Dongsansuk A, Lütz C, Neuner G (2013) Effects of temperature and irradiance on quantum yield of PSII photochemistry and xanthophyll cycle in a tropical and a temperate species. *Photosynthetica*, **51**, 13–21.

Dusenge ME, Duarte AG, Way DA (2019) Plant carbon metabolism and climate change: elevated CO2 and temperature impacts on photosynthesis, photorespiration and respiration. *New Phytologist*, **221**, 32–49.

Ellsworth DS, Reich PB, Naumburg ES, Koch GW, Kubiske ME, Smith SD (2004) Photosynthesis, carboxylation and leaf nitrogen responses of 16 species to elevated pCO2 across four free-air CO2 enrichment experiments in forest, grassland and desert. *Global Change Biology*, **10**, 2121–2138.

Farquhar GD, von Caemmerer S, Berry JA (1980) A biochemical model of photosynthetic CO 2 assimilation in leaves of C 3 species. *Planta*, **149**, 78–90.

Fox J, Weisberg S (2011) An {R} Companion to Applied Regression, Second Edition.

Friedlingstein P, Meinshausen M, Arora VK, Jones CD, Anav A, Liddicoat SK, Knutti R (2013) Uncertainties in CMIP5 Climate Projections due to Carbon Cycle Feedbacks. *Journal of Climate*, **27**, 511–526.

611 Galbraith D, Levy PE, Sitch S, Huntingford C, Cox P, Williams M, Meir P (2010) Multiple
612 mechanisms of Amazonian forest biomass losses in three dynamic global vegetation models
613 under climate change. *New Phytologist*, **187**, 647–665.
614 Ge Z-M, Zhou X, Kellomäki S, Peltola H, Martikainen PJ, Wang KY (2012) Acclimation of
615 photosynthesis in a boreal grass (Phalaris arundinacea L.) under different temperature, CO2,
616 and soil water regimes. *Photosynthetica*, **50**, 141–151.
617 Griffin KL, Tissue DT, Turnbull MH, Whitehead D (2000) The onset of photosynthetic
618 acclimation to elevated CO2 partial pressure in field-grown Pinus radiata D. Don. after 4
619 years. *Plant, Cell & Environment*, **23**, 1089–1098.
620 Hao XY, Han X, Lam SK et al. (2012) Effects of fully open-air [CO 2] elevation on leaf
621 ultrastructure, photosynthesis, and yield of two soybean cultivars. *Photosynthetica*, 1–9.
622 Harley PC, Thomas RB, Reynolds JF, Strain BR (1992) Modelling photosynthesis of cotton
623 grown in elevated CO2. *Plant, Cell & Environment*, **15**, 271–282.
624 Harris I, Jones PD, Osborn TJ, Lister DH (2014) Updated high-resolution grids of monthly
625 climatic observations – the CRU TS3.10 Dataset. *International Journal of Climatology*, **34**,
626 623–642.
627 Harrison MT, Edwards EJ, Farquhar GD, Nicotra AB, Evans JR (2009) Nitrogen in cell walls of
628 sclerophyllous leaves accounts for little of the variation in photosynthetic nitrogen-use
629 efficiency. *Plant, Cell & Environment*, **32**, 259–270.
630 Haxeltine A, Prentice IC (1996) A General Model for the Light-Use Efficiency of Primary
631 Production. *Functional Ecology*, **10**, 551–561.
632 Hikosaka K, Ishikawa K, Borjigidai A, Muller O, Onoda Y (2006) Temperature acclimation of
633 photosynthesis: mechanisms involved in the changes in temperature dependence of
634 photosynthetic rate. *Journal of Experimental Botany*, **57**, 291–302.
635 Hovenden MJ (2003) Photosynthesis of coppicing poplar clones in a free-air CO<emph
636 type="8">2</emph> enrichment (FACE) experiment in a short-rotation forest. *Functional*
637 *Plant Biology*, **30**, 391–400.
638 Huber ML, Perkins RA, Laesecke A et al. (2009) New International Formulation for the
639 Viscosity of H2O. *Journal of Physical and Chemical Reference Data*, **38**, 101–125.
640 Kattge J, Knorr W (2007) Temperature acclimation in a biochemical model of photosynthesis: a
641 reanalysis of data from 36 species. *Plant, Cell & Environment*, **30**, 1176–1190.

642 Kattge J, Diaz S, Lavorel S et al. (2011) TRY–a global database of plant traits. *Global change*
643 *biology*, **17**, 2905–2935.
644 Kattge J, Bönisch G, Díaz S et al. (2020) TRY plant trait database – enhanced coverage and open
645 access. *Global Change Biology*, **26**, 119–188.
646 Keenan TF, Niinemets Ü (2016) Global leaf trait estimates biased due to plasticity in the shade.
647 *Nature Plants*, **3**, 16201.
648 Kitao M, Lei TT, Koike T, Kayama M, Tobita H, Maruyama Y (2007) Interaction of drought and
649 elevated CO2 concentration on photosynthetic down-regulation and susceptibility to
650 photoinhibition in Japanese white birch seedlings grown with limited N availability. *Tree*
651 *Physiology*, **27**, 727–735.
652 Kumarathunge DP, Medlyn BE, Drake JE et al. (2019) Acclimation and adaptation components
653 of the temperature dependence of plant photosynthesis at the global scale. *New Phytologist*,
654 **222**, 768–784.
655 Leakey ADB, Ainsworth EA, Bernacchi CJ, Rogers A, Long SP, Ort DR (2009) Elevated CO2
656 effects on plant carbon, nitrogen, and water relations: six important lessons from FACE.
657 *Journal of experimental botany*, **60**, 2859–2876.
658 Li J-H, Dijkstra P, Hinkle CR, Wheeler RM, Drake BG (1999) Photosynthetic acclimation to
659 elevated atmospheric CO2 concentration in the Florida scrub-oak species Quercus geminata
660 and Quercus myrtifolia growing in their native environment. *Tree Physiology*, **19**, 229–234.
661 Lombardozzi DL, Bonan GB, Smith NG, Dukes JS, Fisher RA (2015) Temperature acclimation
662 of photosynthesis and respiration: A key uncertainty in the carbon cycle-climate feedback.
663 *Geophysical Research Letters*, **42**, 8624–8631.
664 Luo Y, Su B, Currie WS et al. (2004) Progressive Nitrogen Limitation of Ecosystem Responses
665 to Rising Atmospheric Carbon Dioxide. *BioScience*, **54**, 731–739.
666 Maire V, Martre P, Kattge J, Gastal F, Esser G, Fontaine S, Soussana J-F (2012) The
667 Coordination of Leaf Photosynthesis Links C and N Fluxes in C3 Plant Species. *PLOS*
668 *ONE*, **7**, e38345.
669 Maire V, Wright IJ, Prentice IC et al. (2015) Global effects of soil and climate on leaf
670 photosynthetic traits and rates. *Global Ecology and Biogeography*, **24**, 706–717.
671 McKee IF, Woodward FI (1994) The effect of growth at elevated CO2 concentrations on
672 photosynthesis in wheat. *Plant, Cell & Environment*, **17**, 853–859.

McKee IF, Farage PK, Long SP (1995) The interactive effects of elevated CO2 and O3 concentration on photosynthesis in spring wheat. *Photosynthesis Research*, **45**, 111–119.

Medlyn BE (1996) The Optimal Allocation of Nitrogen Within the C_3 Photosynthetic System at Elevated CO_2. *Functional Plant Biology*, **23**, 593–603.

Medlyn BE, Badeck F-W, De Pury DGG et al. (1999) Effects of elevated [CO2] on photosynthesis in European forest species: a meta-analysis of model parameters . *Plant, Cell & Environment*, **22**, 1475–1495.

Mercado LM, Medlyn BE, Huntingford C et al. (2018) Large sensitivity in land carbon storage due to geographical and temporal variation in the thermal response of photosynthetic capacity. *New Phytologist*, **218**, 1462–1477.

Myers DA, Thomas RB, Delucia EH (1999) Photosynthetic capacity of loblolly pine (Pinus taeda L.) trees during the first year of carbon dioxide enrichment in a forest ecosystem. *Plant, Cell & Environment*, **22**, 473–481.

Niinemets Ü, Tenhunen JD (1997) A model separating leaf structural and physiological effects on carbon gain along light gradients for the shade-tolerant species Acer saccharum. *Plant, Cell & Environment*, **20**, 845–866.

Niinemets Ü, Keenan TF, Hallik L (2015) A worldwide analysis of within-canopy variations in leaf structural, chemical and physiological traits across plant functional types. *New Phytologist*, **205**, 973–993.

Norby RJ, Warren JM, Iversen CM, Medlyn BE, McMurtrie RE (2010) CO2 enhancement of forest productivity constrained by limited nitrogen availability. *Proceedings of the National Academy of Sciences*, **107**, 19368–19373.

Oleson KW, Lawrence DM, Bonan GB et al. (2013) *Technical Description of version 4.5 of the Community Land Model (CLM)*. 402 pp.

Onoda Y, Hirose T, Hikosaka K (2009) Does leaf photosynthesis adapt to CO2-enriched environments? An experiment on plants originating from three natural CO2 springs. *New Phytologist*, **182**, 698–709.

Osborne CP, La Roche J, Garcia RL et al. (1998) Does Leaf Position within a Canopy Affect Acclimation of Photosynthesis to Elevated CO2? Analysis of a Wheat Crop under Free-Air CO2Enrichment. *Plant Physiology*, **117**, 1037–1045.

Phillips RP, Meier IC, Bernhardt ES, Grandy AS, Wickings K, Finzi AC (2012) Roots and fungi

accelerate carbon and nitrogen cycling in forests exposed to elevated CO2. *Ecology Letters*, **15**, 1042–1049.

Poorter H, Niinemets Ü, Ntagkas N, Siebenkäs A, Mäenpää M, Matsubara S, Pons T (2019) A meta-analysis of plant responses to light intensity for 70 traits ranging from molecules to whole plant performance. *New Phytologist*, **0**.

Prentice IC, Dong N, Gleason SM, Maire V, Wright IJ (2014) Balancing the costs of carbon gain and water transport: testing a new theoretical framework for plant functional ecology. *Ecology Letters*, **17**, 82–91.

Prentice IC, Liang X, Medlyn BE, Wang Y-P (2015) Reliable, robust and realistic: the three R's of next-generation land-surface modelling. *Atmos. Chem. Phys.*, **15**, 5987–6005.

R Core Team (2019) R: A Language and Environment for Statistical Computing.

Reich PB, Hungate BA, Luo Y (2006) Carbon-Nitrogen Interactions in Terrestrial Ecosystems in Response to Rising Atmospheric Carbon Dioxide. *Annual Review of Ecology, Evolution, and Systematics*, **37**, 611–636.

Rey A, Jarvis PG (1998) Long-term photosynthetic acclimation to increased atmospheric CO2 concentration in young birch (Betula pendula) trees. *Tree Physiology*, **18**, 441–450.

Rogers A (2014) The use and misuse of Vc, max in Earth System Models. *Photosynthesis Research*, **119**, 15–29.

Rogers A, Fischer BU, Bryant J, Frehner M, Blum H, Raines CA, Long SP (1998) Acclimation of Photosynthesis to Elevated CO2under Low-Nitrogen Nutrition Is Affected by the Capacity for Assimilate Utilization. Perennial Ryegrass under Free-Air CO2 Enrichment. *Plant Physiology*, **118**, 683–689.

Rogers A, Medlyn BE, Dukes JS et al. (2017a) A roadmap for improving the representation of photosynthesis in Earth system models. *New Phytologist*, **213**, 22–42.

Rogers A, Serbin SP, Ely KS, Sloan VL, Wullschleger SD (2017b) Terrestrial biosphere models underestimate photosynthetic capacity and CO2 assimilation in the Arctic. *New Phytologist*, **216**, 1090–1103.

Rohatgi A (2017) WebPlotDigitizer.

Sage RF, Kubien DS (2007) The temperature response of C3 and C4 photosynthesis. *Plant, Cell & Environment*, **30**, 1086–1106.

Scafaro AP, Xiang S, Long BM et al. (2017) Strong thermal acclimation of photosynthesis in

tropical and temperate wet-forest tree species: the importance of altered Rubisco content. *Global Change Biology*, **23**, 2783–2800.

Sharwood RE, Crous KY, Whitney SM, Ellsworth DS, Ghannoum O (2017) Linking photosynthesis and leaf N allocation under future elevated CO2 and climate warming in Eucalyptus globulus. *Journal of Experimental Botany*, **68**, 1157–1167.

Sims DA, Luo Y, Seemann JR (1998) Comparison of photosynthetic acclimation to elevated CO2 and limited nitrogen supply in soybean. *Plant, Cell & Environment*, **21**, 945–952.

Singsaas EL, Ort DR, Delucia EH (2004) Elevated CO2 effects on mesophyll conductance and its consequences for interpreting photosynthetic physiology. *Plant, Cell & Environment*, **27**, 41–50.

Smith NG, Dukes JS (2013) Plant respiration and photosynthesis in global-scale models: incorporating acclimation to temperature and CO2. *Global Change Biology*, **19**, 45–63.

Smith NG, Dukes JS (2017a) Short-term acclimation to warmer temperatures accelerates leaf carbon exchange processes across plant types. *Global Change Biology*, **23**, 4840–4853.

Smith NG, Dukes JS (2017b) LCE: Leaf carbon exchange dataset for tropical, temperate, and boreal species of North and Central America. *Ecology*, **98**, 2978.

Smith NG, Dukes JS (2018) Drivers of leaf carbon exchange capacity across biomes at the continental scale. *Ecology*, **99**, 1610–1620.

Smith NG, Malyshev SL, Shevliakova E, Kattge J, Dukes JS (2016) Foliar temperature acclimation reduces simulated carbon sensitivity to climate. *Nature Clim. Change*, **6**, 407–411.

Smith NG, Lombardozzi D, Tawfik A, Bonan G, Dukes JS (2017) Biophysical consequences of photosynthetic temperature acclimation for climate. *Journal of Advances in Modeling Earth Systems*, **9**, 536–547.

Smith NG, Keenan TF, Prentice IC et al. (2019) Global photosynthetic capacity is optimized to the environment. *Ecology Letters*, **22**, 506–517.

Terrer C, Vicca S, Hungate BA, Phillips RP, Prentice IC (2016) Mycorrhizal association as a primary control of the CO2 fertilization effect. *Science*, **353**, 72–74.

Terrer C, Vicca S, Stocker BD et al. (2018) Ecosystem responses to elevated CO2 governed by plant–soil interactions and the cost of nitrogen acquisition. *New Phytologist*, **217**, 507–522.

Thornton PE, Lamarque J-F, Rosenbloom NA, Mahowald NM (2007) Influence of carbon-

nitrogen cycle coupling on land model response to CO2 fertilization and climate variability. *Global Biogeochemical Cycles*, **21**, GB4018.

Tissue DT, Griffin KL, Ball JT (1999) Photosynthetic adjustment in field-grown ponderosa pine trees after six years of exposure to elevated CO2. *Tree Physiology*, **19**, 221–228.

Togashi HF, Atkin OK, Bloomfield KJ et al. (2018a) Functional trait variation related to gap dynamics in tropical moist forests: a vegetation modelling perspective. *Perspectives in Plant Ecology, Evolution and Systematics*.

Togashi HF, Prentice IC, Atkin OK, Macfarlane C, Prober SM, Bloomfield KJ, Evans BJ (2018b) Thermal acclimation of leaf photosynthetic traits in an evergreen woodland, consistent with the coordination hypothesis. *Biogeosciences*, **15**, 3461–3474.

Turnbull MH, Tissue DT, Griffin KL, Rogers GND, Whitehead D (1998) Photosynthetic acclimation to long-term exposure to elevated CO2 concentration in Pinus radiata D. Don. is related to age of needles. *Plant, Cell & Environment*, **21**, 1019–1028.

Verheijen LM, Aerts R, Brovkin V, Cavender-Bares J, Cornelissen JHC, Kattge J, van Bodegom PM (2015) Inclusion of ecologically based trait variation in plant functional types reduces the projected land carbon sink in an earth system model. *Global Change Biology*, **21**, 3074–3086.

Walker AP, Beckerman AP, Gu L et al. (2014) The relationship of leaf photosynthetic traits – Vcmax and Jmax – to leaf nitrogen, leaf phosphorus, and specific leaf area: a meta-analysis and modeling study. *Ecology and Evolution*, **4**, 3218–3235.

Wang H, Prentice IC, Keenan TF et al. (2017a) Towards a universal model for carbon dioxide uptake by plants. *Nature Plants*, **3**, 734–741.

Wang H, Harrison S, Prentice I et al. (2017b) The China Plant Trait Database: towards a comprehensive regional compilation of functional traits for land plants. *Ecology*, **99**, 500–500.

Warren JM, Jensen AM, Medlyn BE, Norby RJ, Tissue DT (2015) Carbon dioxide stimulation of photosynthesis in Liquidambar styraciflua is not sustained during a 12-year field experiment. *AoB PLANTS*, **7**, plu074–plu074.

Weedon GP, Balsamo G, Bellouin N, Gomes S, Best MJ, Viterbo P (2014) The WFDEI meteorological forcing data set: WATCH Forcing Data methodology applied to ERA-Interim reanalysis data. *Water Resources Research*, **50**, 7505–7514.

797 Wright IJ, Reich PB, Westoby M (2003) Least-cost input mixtures of water and nitrogen for
798 photosynthesis. *The American Naturalist*, **161**, 98–111.
799 Yamori W, Hikosaka K, Way DA (2014) Temperature response of photosynthesis in C3, C4, and
800 CAM plants: temperature acclimation and temperature adaptation. *Photosynthesis Research*,
801 **119**, 101–117.
802 Yong Z-H, Chen G-Y, Zhang D-Y, Chen Y, Chen J, Zhu J-G, Xu D-Q (2007) Is photosynthetic
803 acclimation to free-air CO2 enrichment (FACE) related to a strong competition for the
804 assimilatory power between carbon assimilation and nitrogen assimilation in rice leaf?
805 *Photosynthetica*, **45**, 85–91.
806 Yu J, Chen L, Xu M, Huang B (2012) Effects of Elevated CO2 on Physiological Responses of
807 Tall Fescue to Elevated Temperature, Drought Stress, and the Combined Stresses. *Crop*
808 *Science*, **52**, 1848–1858.
809 Zhao D, Reddy KR, Kakani VG, Mohammed AR, Read JJ, Gao W e. i. (2004) Leaf and canopy
810 photosynthetic characteristics of cotton (Gossypium hirsutum) under elevated CO2
811 concentration and UV-B radiation. *Journal of Plant Physiology*, **161**, 581–590.
812 Ziska LH, Hogan KP, Smith AP, Drake BG (1991) Growth and photosynthetic response of nine
813 tropical species with long-term exposure to elevated carbon dioxide. *Oecologia*, **86**, 383–
814 389.
815 Zuur AF, Ieno EN, Walker NJ, Saveliev AA, Smith GM (2009) *Mixed effects models and*
816 *extensions in ecology with R. Gail M, Krickeberg K, Samet JM, Tsiatis A, Wong W, editors*.
817 New York, NY, USA.
818

Table 1. Parameter values used for the observation-based acclimation formulations of Kattge and Knorr (2007) and Kumarathunge *et al*. (2019) as well as the enzyme kinetic (i.e., unacclimated) model used in the model-data comparisons*

	V_{cmax}			J_{max}		
	H_a	ΔS	k_{25}	H_a	ΔS	k_{25}
Kattge and Knorr (2007)	71513	668.39-1.07*T_{acc}	1	49884	659.7-0.7*T_{acc}	(2.59-0.035*T_{acc})*$V_{cmax,25}$
Kumarathunge et al. (2019)	48700+0.82*T_{acc}	662-1.31*T_{acc}	1	40710	667.3-1.34*T_{acc}	(2.56-0.0375*T_{acc})*$V_{cmax,25}$
Enzyme kinetic model	71513	641.64	1	49884	642.2	1

*Key: H_a = activation energy (J mol^{-1}), ΔS = entropy term that that characterizes the changes in reaction rate caused by substrate concentration (J mol^{-1} K^{-1}), and k_{25} (μmol m^{-2} s^{-1}) is the rate of V_{cmax} or J_{max} at at 25°C ($V_{cmax,25}$ and $J_{max,25}$, respectively). Values from Kumarathunge *et al*. (2019) were based on the values reported for the "mature plants in native environment" dataset (Kumarathunge *et al.*, 2019). Values for the enzyme kinetic model were taken from static, mean parameter values (computed at T_{acc} = 25°C) from Kattge and Knorr (2007).

Table 2. Observed, kinetic, and optimal slope of the natural log transformed values of J_{max}/V_{cmax}, V_{cmax}, and J_{max} to acclimated temperature in temperature acclimation-only growth chamber manipulations*

		Slope	95% CI	Intercept	95% CI
J_{max}/V_{cmax}	Kinetic	-0.028[a]	<0.001	-	-
	Optimal	-0.051[b]	0.001	1.990	0.038
	Smith & Dukes (2017)	-0.048[b]	0.012	1.750	0.307
	Scafaro et al. (2017)	-	-	-	-
V_{cmax}	Kinetic	0.083[a]	0.004	-	-
	Optimal	0.048[b]	<0.001	4.404	0.010
	Smith & Dukes (2017)	0.080[a,b]	0.044	1.455	1.133
	Scafaro et al. (2017)	0.073[a]	0.008	-1.757	0.200
J_{max}	Kinetic	0.055[a]	0.004	-	-
	Optimal	-0.002[b]	0.002	6.394	0.047
	Smith & Dukes (2017)	0.032[a,b]	0.044	3.205	1.138
	Scafaro et al. (2017)	-	-	-	-

*The temperature response slope ($°C^{-1}$) was derived by fitting a linear model to the natural log of data predicted from the kinetic model (Table 1), the optimal photosynthesis model (Optimal; see Methods) and observed by Smith and Dukes (2017a) and Scafaro *et al*. (2017). Superscripts on slope values indicate slopes with overlapping 95% confidence intervals within each variable grouping (i.e., J_{max}/V_{cmax}, V_{cmax}, and J_{max}).

Table 3. Observed, kinetic, and optimal slope of the natural log transformed values of J_{max}/V_{cmax}, V_{cmax}, and J_{max} to acclimated temperature in global observations and global observation-based forumations (Kattge & Knorr, 2007; Kumarathunge *et al.*, 2019)*

		Slope	95% CI	Intercept	95% CI
J_{max}/V_{cmax}	Kinetic	-0.031[a]	<0.001	0.771	0.006
	Optimal	-0.041[b]	<0.001	1.777	0.004
	Kattge & Knorr (2007)	-0.041[b]	0.002	1.577	0.028
	Kumarathunge et al. (2019)	-0.032[a]	0.001	1.271	0.010
	Global dataset	-0.046[c]	0.002	1.656	0.036

V_{cmax}	Kinetic	0.100[a]	0.002	-2.508	0.032
	Optimal	0.061[e]	0.001	4.217	0.014
	Kattge & Knorr (2007)	0.088[b]	0.001	-2.202	0.015
	Kumarathunge et al. (2019)	0.069[d]	0.001	-1.734	0.015
	Global dataset	0.082[c]	0.003	1.686	0.061
J_{max}	Kinetic	0.069[a]	0.001	-1.737	0.026
	Optimal	0.020[d]	0.001	5.994	0.014
	Kattge & Knorr (2007)	0.046[b]	0.001	-0.624	0.017
	Kumarathunge et al. (2019)	0.038[c]	0.001	-0.463	0.026
	Global dataset	0.037[c]	0.003	3.306	0.072

*The temperature response slope ($°C^{-1}$) was derived by fitting a linear model to the natural log of data predicted from the kinetic model (Table 1), optimality model (Optimal; see Methods), the global observational dataset (Global dataset; Table S2), and the global observation-based formulations (Kattge & Knorr, 2007; Kumarathunge *et al.*, 2019). Superscripts on slope values indicate slopes with overlapping 95% confidence intervals within each variable grouping (i.e., J_{max}/V_{cmax}, V_{cmax}, and J_{max}).

Table 4. Analysis of variance results examining variables that explain bias in observed versus modeled responses to elevated CO_2*

		J_{max}/V_{cmax}		V_{cmax}		J_{max}	
	Df	*F*	*P*	*F*	*P*	*F*	*P*
Methodology	3	2.25	0.088	1.66	0.179	1.18	0.324
Nitrogen acquisition	3	2.85	**0.042**	1.14	0.335	2.49	0.066
Temperature	1	0.23	0.632	2.19	0.142	0.29	0.592
Vapor pressure deficit	1	0.24	0.629	1.35	0.247	0.07	0.786
Light availability	1	0.08	0.781	0.16	0.686	0.68	0.412
Elevation	1	1.70	0.196	0.01	0.939	0.00	0.992
Residuals	89						

*Variable key: Methodology = methodology used for elevated CO_2 experiments (FACE, OTCs, WTCs, or CEs); Nitrogen acquisition = nitrogen fertilization or potential symbiosis used to acquire nitrogen (arbuscular mycorrhizae only, ectomycorrhizae only, or nitrogen fixating

850 bacteria); Temperature = growing season mean temperature from 1901-2015; Vapor pressure
851 deficit = growing season mean vapor pressure deficit from 1901-2015; Light availability =
852 growing season mean PAR from 1901-2015; Elevation = elevation of the site. P-values less than
853 0.05 are bolded.

Table 5. Observed and optimal slope of the response of natural log transformed values of J_{max}/V_{cmax}, V_{cmax}, and J_{max} to atmospheric CO_2 in CO_2 manipulation experiments*

		AM			EM			NF			Fertilized		
		n	Slope	95% CI	n	Slope	95% CI	n	Slope	95% CI	n	Slope	95% CI
J_{max}/V_{cmax}	Optimal	44	0.0090[a]	0.0004	43	0.0071[a]	0.0004	9	0.0090[a]	0.0014	4	0.0099[a]	0.0018
	Observed	44	0.0010[b]	0.0015	43	0.0011[b]	0.0026	9	0.0091[a]	0.0099	4	0.0015[a]	0.0065
V_{cmax}	Optimal	60	-0.0065[a]	0.0003	46	-0.0053[a]	0.0003	12	-0.0065[a]	0.0008	8	-0.0071[a]	0.0010
	Observed	60	-0.0042[a]	0.0021	46	-0.0059[a]	0.0022	12	-0.0096[a]	0.0110	8	-0.0098[a]	0.0108
J_{max}	Optimal	44	0.0025[a]	0.0002	43	0.0018[a]	0.0001	9	0.0025[a]	0.0006	4	0.0028[a]	0.0008
	Observed	44	-0.0029[b]	0.0020	43	-0.0049[b]	0.0030	9	0.0032[a]	0.0043	4	0.0008[a]	0.0034

The CO_2 response slope (Pa^{-1}) was derived by fitting a linear model to the natural log of data predicted from the optimality model (Optimal; see Methods) and observed in the CO_2 manipulation dataset (Observed; Table S2). Data are separated by nitrogen acquisition type: arbuscular mycorrhizal associating species (AM), ectomycorrhizal associating species (EM), and nitrogen fixing bacteria associating species (NF), and fertilized species (orange). Superscripts on slope values indicate slopes with overlapping 95% confidence intervals within each variable (i.e., J_{max}/V_{cmax}, V_{cmax}, and J_{max}) by nitrogen acquisition (i.e., AM, EM, NF, and Fertilized) grouping.

Figure Legends

Figure 1. Temperature response of photosynthetic biochemistry from temperature manipulation studies. Temperature response of (a) J_{max}/V_{cmax}, (b) V_{cmax}, and (c) J_{max} observed in the Smith and Dukes (2017a) dataset (Sm2017; black line and transparent black dots), the Scafaro *et al*. (2017) dataset (Sc2017; purple line), as well as that predicted by optimality (blue line) and enzyme kinetics (red line). Solid lines indicate fits to observed data and dotted lines indicate modeled responses. To facilitate comparisons, all lines and points are standardized to 1 at 25°C by dividing values by the value predicted at 25°C from the linear model fit between temperature and the natural log transformed rate.

Figure 2. Temperature response of photosynthetic biochemistry from global observations. Temperature response of (a) J_{max}/V_{cmax}, (b) V_{cmax}, and (c) J_{max} observed in the global dataset (black line and transparent black dots), the Kattge and Knorr observation-based formulation (green dashed line), the Kumarathunge *et al*. (2019) observation-based formulation (orange dashed line), as well as that predicted by optimality (blue dotted line) and enzyme kinetics (red dotted line). The solid line indicates the fit to observed data, the dashed lines indicate responses from observation-based formulations, and the dotted lines indicate modeled responses. To facilitate comparisons, all lines and points are standardized to 1 at 25°C by dividing values by the value predicted at 25°C from the linear model fit between temperature and the natural log transformed rate. Standardized observation values greater than 4 were omitted to better visualize the differences between lines (n = 10, 16, and 5 for J_{max}/V_{cmax}, V_{cmax}, and J_{max}, respectively).

Figure 3. CO_2 response of photosynthetic biochemistry from CO_2 manipulation studies. Slope of the response of natural log transformed values of (a) J_{max}/V_{cmax}, (b) V_{cmax}, and (c) J_{max} to atmospheric CO_2 (Δ; Pa^{-1}) for each species in each of the elevated CO_2 experiments reviewed (115 total responses; exes) and predicted from optimality (circles). Boxes indicate median, first quartile, and third quartile of the observed data. Whiskers are the furthest data point, no further than 1.5 * the inner quartile range. Data are separated by nitrogen acquisition type: arbuscular mycorrhizal associating species (AM; blue), ectomycorrhizal associating species (EM; purple), and nitrogen fixing bacteria associating species (NF; red), and fertilized species (orange).

Figure 4. Simulated photosynthetic nitrogen (N) under different conditions. The simulated response of photosynthetic N to temperature (different coloration) and atmospheric CO_2 (x-axis) under a low (solid line; 1 kPa) and high (dotted line; 6 kPa) vapor pressure deficit (VPD) environment. Photosynthetic N was determined by adding simulated Rubisco N to bioenergetic N, computed from optimal V_{cmax} and J_{max} simulations (see Methods). All values were standardized to 1 at the value simulated at 25°C, 400 μmol mol^{-1} CO_2, and 1 kPa VPD. This value is indicated with circle cross.

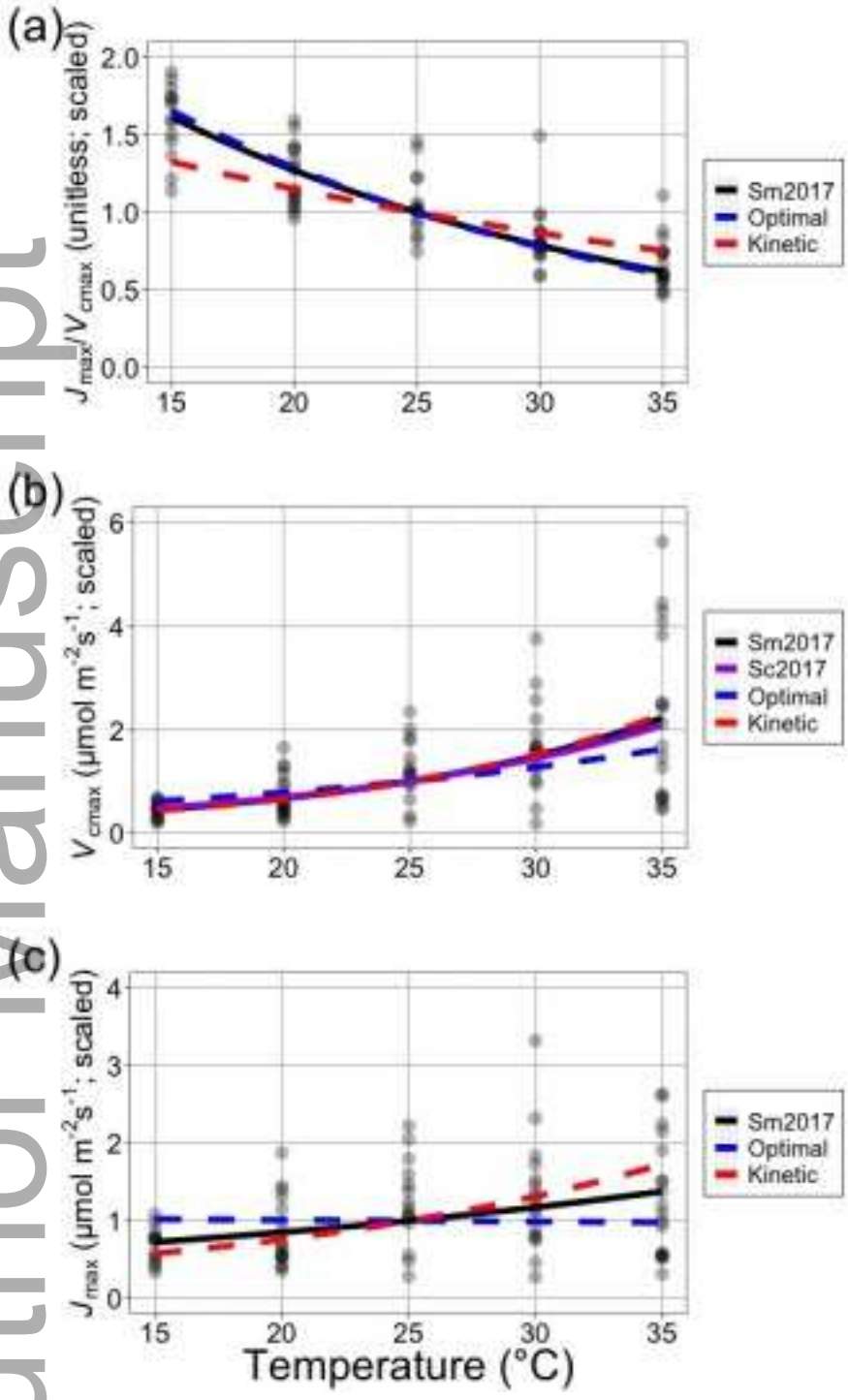

gcb_15212_f1.jpeg

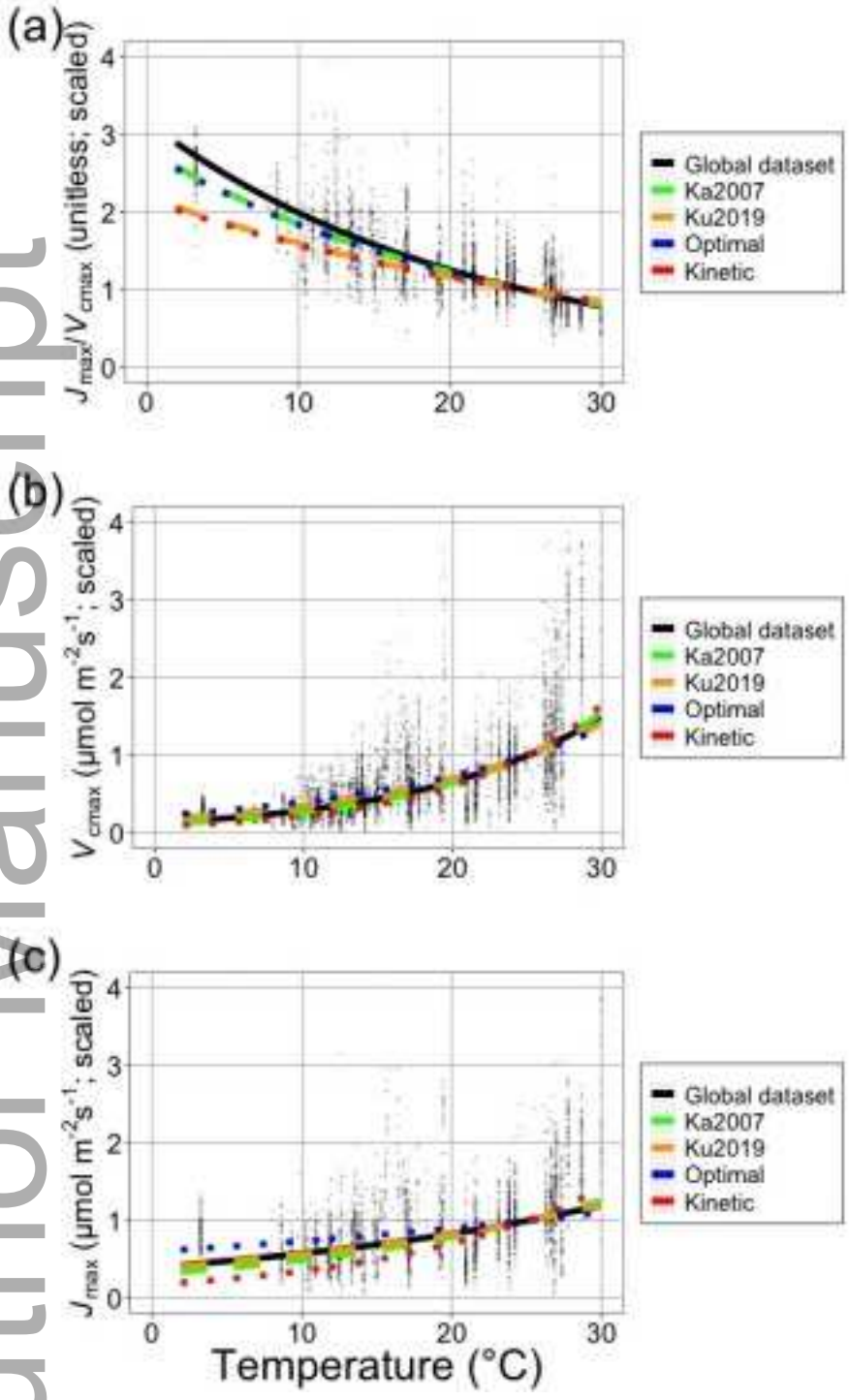

gcb_15212_f2.jpeg

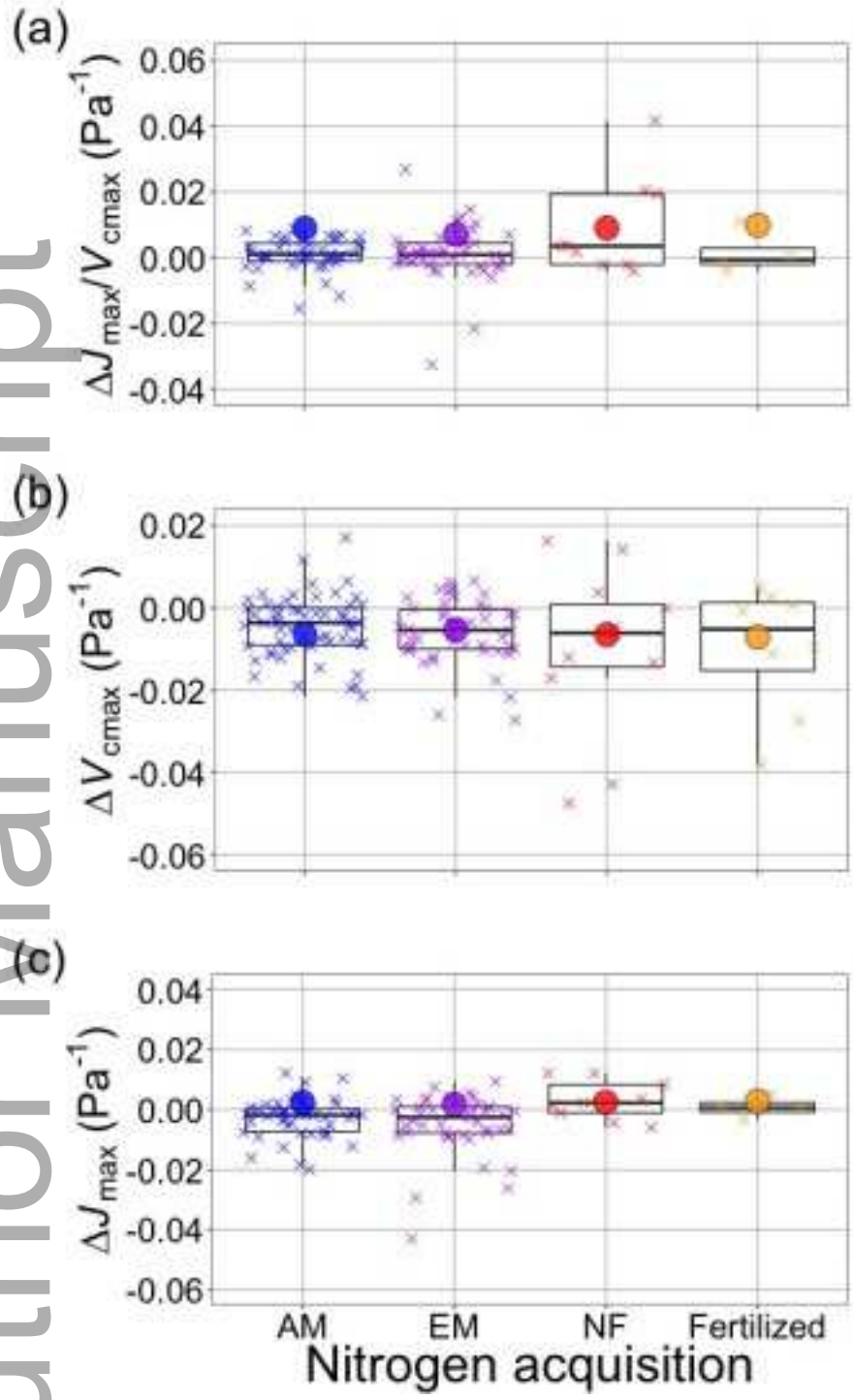

gcb_15212_f3.jpeg

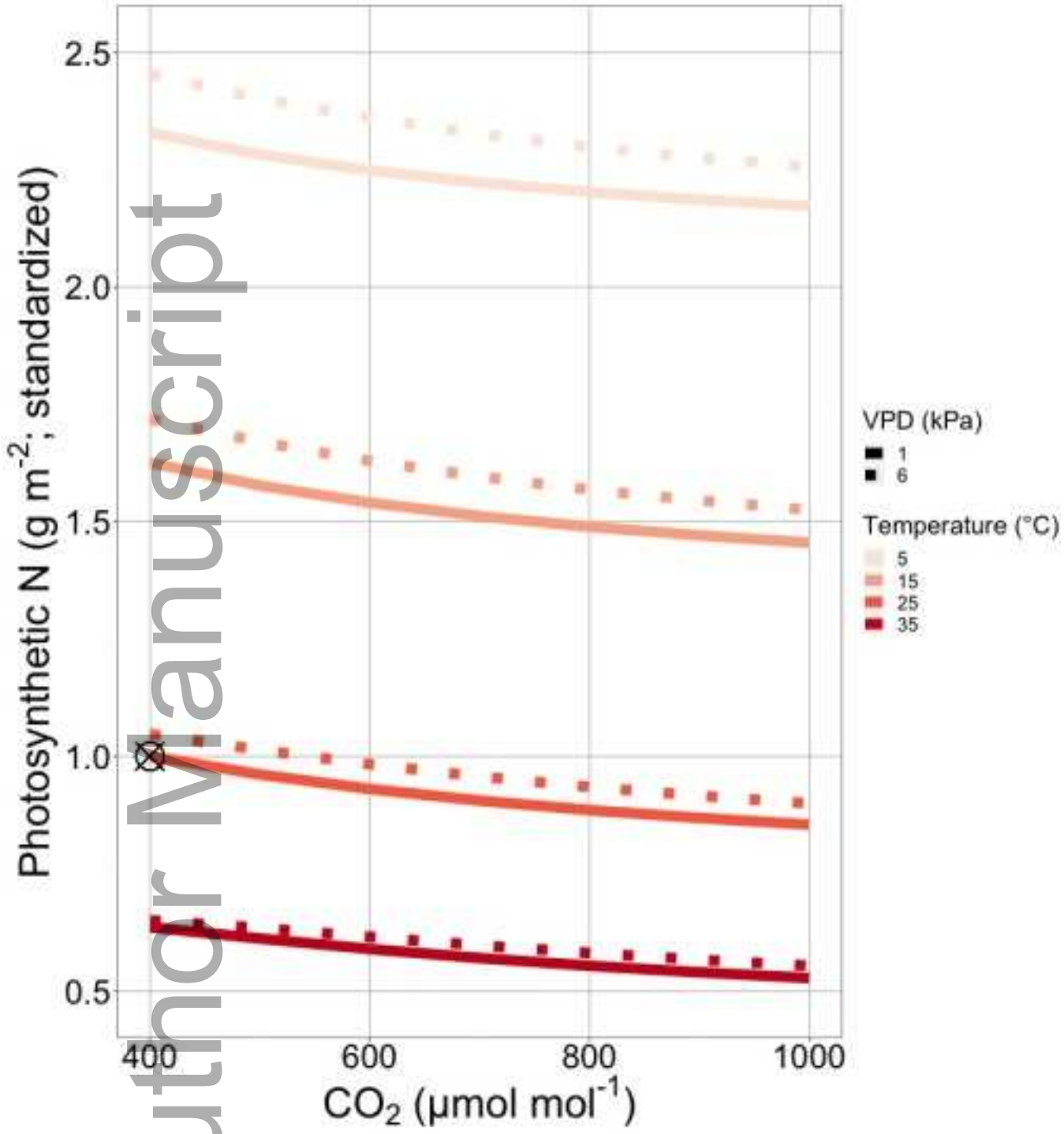

gcb_15212_f4.jpeg